05,08

Structural and superconducting properties of tungsten and iridium films for low-temperature microcalorimeters

© M.N. Drozdov[1], V.M. Daniltsev[1], E.A. Arkhipova[1], O.I. Khrykin[1], P.A. Yunin[1], A.V. Gordeeva[2], V.Yu. Safonova[2], D.A. Pimanov[2], A.L. Pankratov[1,2]

[1] Institute for Physics of Microstructures, Russian Academy of Sciences, Nizhny Novgorod, Russia
[2] Alekseev State Technical University, Nizhny Novgorod, Russia

E-mail: drm@ipm.sci-nnov.ru

Received April 18, 2024
Revised April 18, 2024
Accepted May 8, 2024

The deposition technology and the basic properties of thin layers of tungsten and iridium, promising for the creation of superconducting low-temperature microcalorimeters in the temperature range from 15 to 100 mK, are investigated. Superconducting layers of the α-phase of tungsten with a low superconducting transition temperature $T_c \sim 15$ mK and superconducting iridium layers with $T_c \sim 170$ mK have been obtained, which can serve as the basis for the formation of bilayers with a superconducting transition temperature in the range 15−100 mK.

Keywords: tungsten, iridium, superconductivity, bolometers, X-ray diffractometry, secondary ion mass spectrometry.

DOI: 10.61011/PSS.2024.07.58973.44HH

1. Introduction

This paper outlines the results of study of deposition technologies and main characteristics of thin layers of tungsten and iridium. The purpose of this study is to obtain the superconducting layers with a temperature of superconducting junction (T_c) from 10 to 100 mK and drastic transition $\Delta T_c < 1$ mK to design the single and multi-pixel microcolorimeters on their basis [1]. There are no such superconducting materials that cover this range of critical temperatures, therefore, two approaches are deemed possible. First approach implies the use of metals with several allotropic modifications and different critical temperatures. In this paper we'll consider tungsten as an example of such metals. Tungsten has two lattice modifications: a body-centered cubic lattice, the so called α-W with $T_c = 12-15$ mK (according to various sources) and a primary cubic lattice, phase A15, β-W with $T_c = 1-4$ K. The appropriate deposition conditions allow fabricating the tungsten films with various allotropic modifications, and, as a consequence, vary the temperature T_c [2–5]. The second approach is based on the use of two- or three-layer systems consisting of alternating layers of the superconducting and normal metals, where overall critical temperature will be reduced relatively to T_c of a bulk superconducting material as a result of proximity effect [6–9]. Paper [10] describes modeling of a critical temperature for the two- and three-layer structures in conditions of proximity effect. In this paper we will use iridium as a superconducting metal with temperature T_c of 120 mK for a bulk material. Only single-layer iridium films will be considered in this paper to define optimal conditions for superconducting structures formation; the bi-layers will be a separate matter considered in another paper. Tungsten and iridium were selected not only because of their critical temperatures, but also due to their chemical stability, as well as absence of inter-layer reaction diffusion.

2. Experimental procedure

Chemical vapor-phase deposition (CVD) method was used to obtain the tungsten films. In our opinion, this method is the most flexible one and allows varying a whole lot of parameters to get the best characteristics of the tungsten films. It should be noted that this method was not used before to get the superconducting tungsten films. Two metalorganic vapor phase epitaxy (MOVPE) systems were used — Epiquip VP-502 RP with a horizontal reactor and original MOVPE growth system with a vertical reactor. W layers were deposited from the tungsten hexafluoride (WF_6) in hydrogen flow. Iridium layers were grown by method of electron-beam sputtering on Amod 206 system. W and Ir layers were analyzed using methods of X-ray diffraction (XRD), small-angle reflectometry (XRR) and secondary ion mass-spectrometry (SIMS). Studies with XRR method enable us to define the thickness, roughness and density of layers, XRD method defines the phase composition of layers, in particular, for the tungsten layers — presence of α and β phases, depending on the growth temperature. SIMS method allows to define the elements of the layers, its profile across the layer thickness, and study the layer−substrate junction areas. Resistivity of layers was defined by a

4-probe method, critical temperature of the superconducting junction was measured in the closed-loop dilution cryostat with limiting temperature of up to 10–15 mK.

3. Results on the study of tungsten layers growth

Figure 1 shows the results of X-ray diffraction analysis of three samples of tungsten grown at different temperatures.

Figure 1 illustrates that in H1030 structure with tungsten deposition temperature $T_{Gr} = 600°C$ the α-phase is observed, in E1130 structure ($T_{Gr} = 420°C$) — $\alpha + \beta$-phases are observed, and in E1525 structure ($T_{Gr} = 380°C$) — β-phase of tungsten can be registered. Tungsten layers in these structures were 200 nm thick.

Figure 2 illustrates the profiles of tungsten and major impurities distribution in H1030 structure with depth on the sapphire substrate; these profiles were obtained by SIMS method. Measurements were carried out with sputtering of cesium ions, electronegative elements having the highest sensitivity.

In H1030 structure the main impurities are fluorine and oxygen, their concentration doesn't exceed 10^{19} at $\cdot$ cm^{-3}. In E1130 and E1525 structures, grown at lower temperatures, the concentration of fluorine and oxygen impurities increased drastically because of incomplete decomposition of WF_6 precursor with CVD growth, E1525 structure was a compound of W + F + O.

Figure 3 illustrates the morphology of tungsten layers grown at different temperatures measured using the atomic-force microscope.

Figure 4 shows the lateral size distribution histograms for the clusters on the surface of tungsten layers grown at different temperatures, obtained from Figure 3.

From Figure 3 and 4 we may see that a range of growth temperatures 600–650°C can be identified where solid films grow with minimal lateral size of clusters with its average value of 17 nm. At lower temperature of 500°C the clusters of larger size were observed with value varying from 60 to 110 nm. If growth temperature higher than 650°C was used it significantly impaired the surface morphology. At 700°C a bimodal distribution of sizes is observed with characteristic values 20 and 35 nm.

Figure 5 shows the current-voltage curves of H1030 sample measured at various temperatures. The current-voltage curves for H1030 structure in Figure 5 demonstrate the occurrence of critical current at a temperature of 14.7 mK which illustrates transition to a superconducting state. It shall be noted that cryostat limiting temperature is near 15 mK, therefore, we cannot measure the ratio of R versus T in this temperature area.

Thus, in H1030 structure with α-phase of tungsten the transition to superconducting state is observed at $T_c = 14.7$ mK. In E1130 structure $\alpha + \beta$-phase W transition to the superconducting state was observed at $T_c \sim 100$ mK.

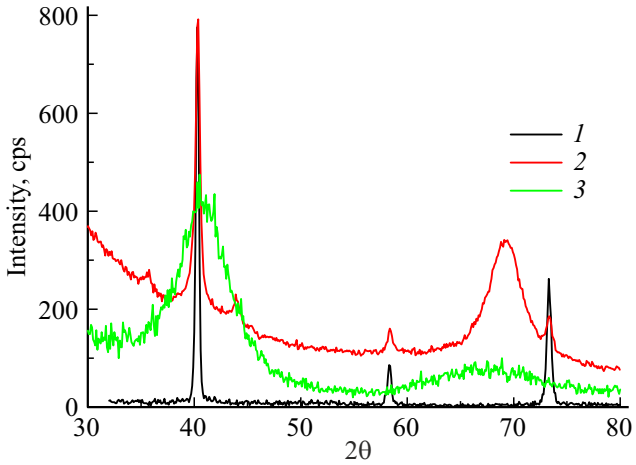

Figure 1. X-ray diffraction patterns of three samples of tungsten grown at different temperatures: *1* — 600, *2* — 420, *3* — 380°C. Intensity of № *2* curve is reduced 10 times.

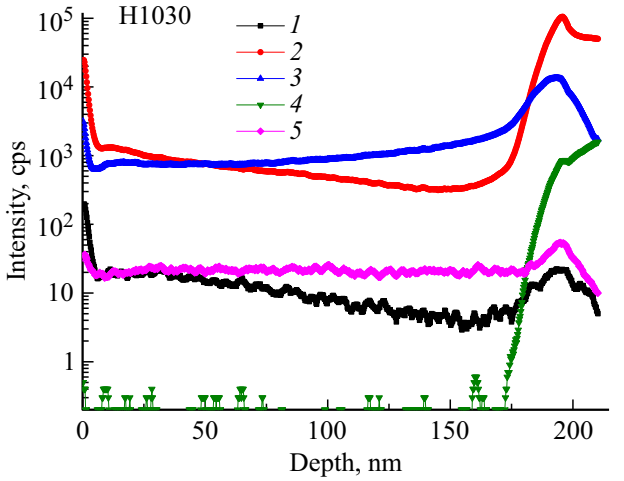

Figure 2. Profiles of tungsten and major impurities distribution in H1030 structure with depth. *1* — C, *2* — O, *3* — F, *4* — Al, *5* — W.

For E1525 sample with β crystalline phase transition to superconducting state occurred between 5 and 3.2 K. At room temperature the resistivity of α-W layer in H1030 structure was $5.6 \cdot 10^{-6}$ Ohm $\cdot$ cm, which is close to table data for bulk tungsten layers. For E1130 and E1525 structures with other tungsten phases the resistivity increased drastically and exceeded $30 \cdot 10^{-6}$ Ohm $\cdot$ cm. However, in papers [2–5] tungsten layers were deposited using magnetron sputtering, yet, the best temperature range for layers growth α-W for this method also was 600–650°C.

4. Results on the study of iridium layers growth

In the first studies [6] for the fabrication of iridium-aurum bi-layers for microcalorimeters the temperature 500–600°C

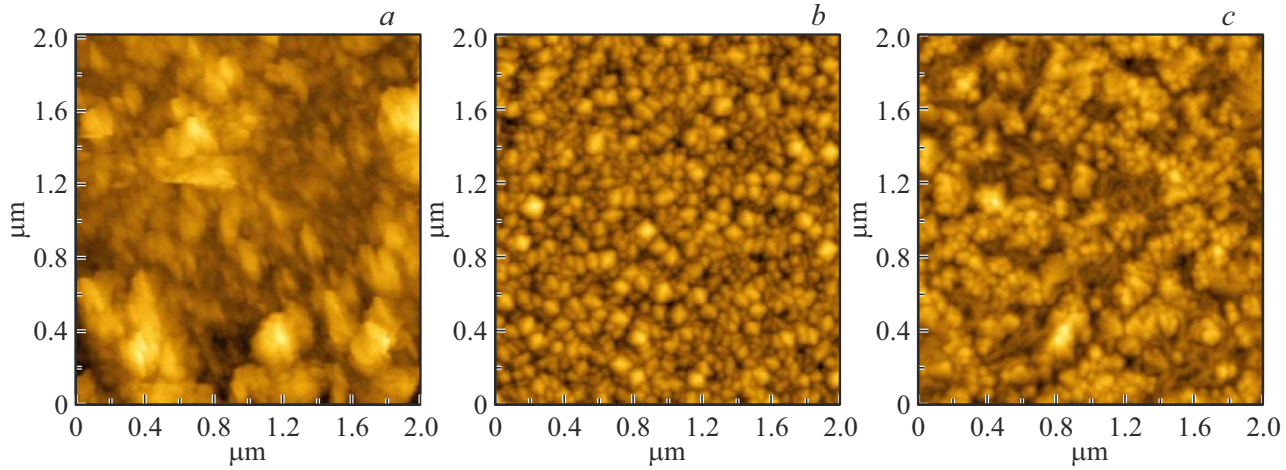

Figure 3. Morphology of tungsten layers surface grown at temperatures: *a* — 500, *b* — 650, *c* — 700°C.

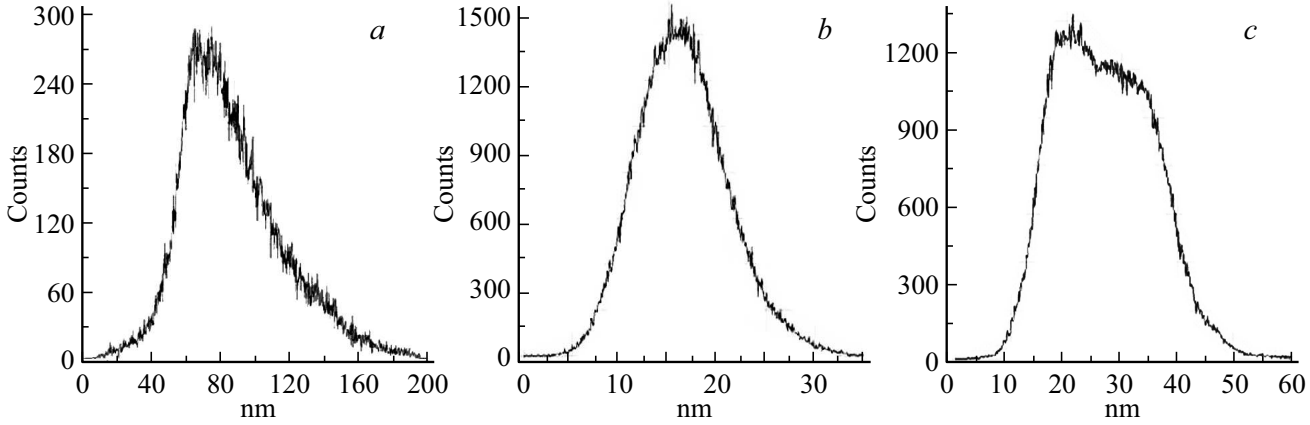

Figure 4. Lateral size histograms of clusters on the surface of tungsten layers grown at temperatures: *a* — 500, *b* — 650, *c* — 700°C.

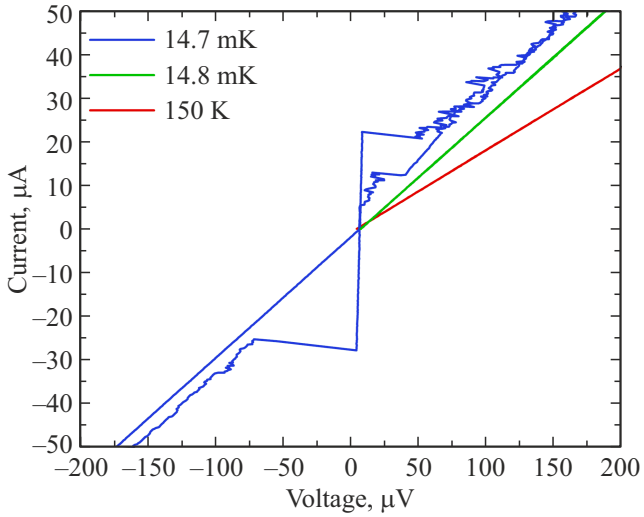

Figure 5. Current-voltage curves for H1030 structure at temperatures of 150, 14.8 and 14.7 mK.

was used for iridium layers growth. However, in later studies [7,8] iridium layers were deposited at room temperature. Deposition of iridium layers at room temperature is a convenient and feasible method that can be applied in further micro-bridges formation processes by method of photolithography without the need for iridium layer etching, since the photoresists for an „explosion-type“ lithography will not deteriorate during iridium deposition.

In this study the layers of iridium were deposited at room temperature. Thickness of iridium layers turned out to be the major parameter for the superconducting properties. Figure 6 illustrates the small-angle X-ray reflectometry curves for three structures with different iridium layers thickness.

Processing of curves shown in Figure 6 by matching the designed layer model curve with the measured one allows to define the thickness and density of layers. These values are given in the table.

Figure 7 illustrates the profiles of iridium and major impurities distribution in A1117 structure with depth obtained by SIMS method.

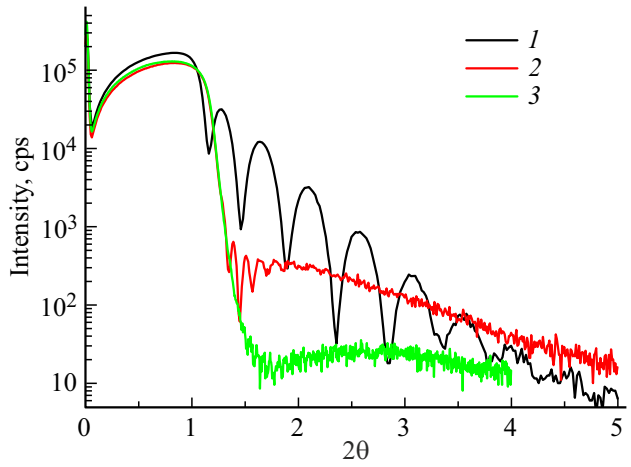

Figure 6. Small-angle X-ray reflectometry curves for three structures with different iridium layers thickness. *1* — D7, *2* — A1117, *3* — A1133.

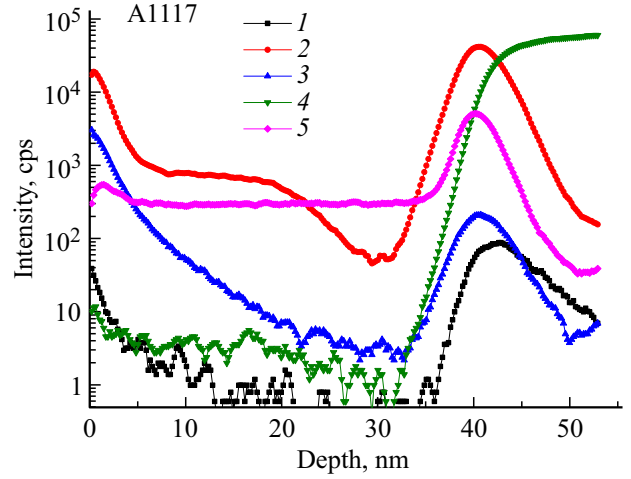

Figure 7. Profiles of tungsten and major impurities distribution in A1117 structure with depth.*1* — C, *2* — O, *3* — CN, *4* — Si, *5* — Ir.

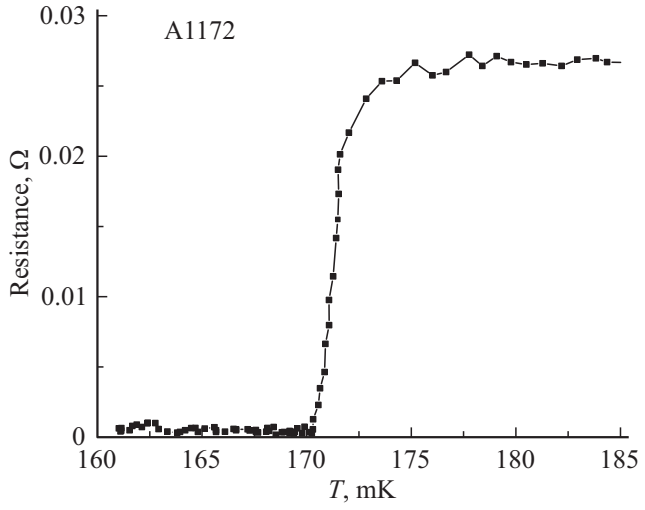

Figure 8. Graph of $R(T)$ superconducting transition in A1172 structure on silicon substrate.

Values of thickness, density and resistivity of iridium layers

Sample	Thickness, nm	Specific density $g \cdot cm^{-3}$	ρ, Ohm · cm
D7	15	16.6	$1.3 \cdot 10^{-4}$
A1117	42.5	22.5	$7.5 \cdot 10^{-6}$
A1133	94	22.5	$6.2 \cdot 10^{-6}$
A1172	135	19.8	$5 \cdot 10^{-5}$

Figure 7 demonstrates that oxygen is the major impurity in A1117 structure. In the layer volume its concentration doesn't exceed 10^{19} at $\cdot$ cm^{-3}, and greatly increases near the layer of junction with silicon substrate. Near the structure surface in a 5 nm thick layer high concentration of nitrogen is observed at $5 \cdot 10^{19}$ at $\cdot$ cm^{-3} level. Note that, because of low sensitivity of SIMS method to elemental nitrogen, in Figure 7 a cluster secondary ion CN is shown that has a much higher intensity. Moreover, from Figure 7 it follows that no distinct diffusion of silicon into iridium layer occurs. If A1117 structure is annealed at a temperature of 900°C the concentration of impurities is decreased, while diffusion of silicon also doesn't occur. This indicates the absence of iridium silicide after annealing which is reported in literature for a slightly higher temperature [11] In this regard, the after-growth annealing is considered an additional opportunity to control the iridium layers properties.

Values of thickness, density and resistivity of iridium layers are given in the Table.

Measurements of the superconducting properties of the grown structures of iridium demonstrated that superconductivity is observed only for the thickest iridium layer in A1172 structure. Figure 8 shows the graph of superconducting transition $R(T)$ of iridium film A1172. The measuring current was 0.2 μA. Figure 8 illustrates that critical temperature T_c in A1172 sample is 171 mK, junction width is about 1 mK.

5. Discussion

The obtained results demonstrate that unlike tungsten layers the parameters of iridium grown layers do not allow to forecast their superconducting capabilities. The table shows that the higher is the thickness of iridium layers 14–45–94 nm the lower is the resistivity which is quite common for thin films. Density of iridium layers reach the table values for a bulk material with a thickness of 45 nm already. However, with further growth of the film thickness to 135 nm the resistivity increases, while density slightly goes down. At the same time, from all given samples only A1172 sample is featuring a property of superconducting transition. These data contradict the established opinion on requirements to the superconducting properties of various metals — for example [2,3]. According to these papers, the closer the layer resistivity at room temperature to the table

resistivity value for bulky samples of this material, the more likely that a superconductivity will occur in this sample. The obtained contradictions can be associated with the stresses occurring in lattice of thinner layers of iridium on the silicon and sapphire substrates and increasing when the substrates are cooled to a temperature below several Kelvins. For the thin tungsten layers this effect was observed with the help of X-ray diffraction measurements at low temperatures [4].

It shall be also emphasized that one of the target parameters in design of a superconducting junction microcalorimeter is the thickness of tungsten or iridium layer below 100 nm which allows reducing the thermal capacity and increasing the sensitivity of microcalorimeters. However, in this paper we considered the thickness of tungsten layers 200 nm which enabled us to more clearly demonstrate the influence of growth parameters on the structural and superconducting properties of W layers. Later these studies will be focused on the growth of thinner tungsten layers and detailed study of lattice stresses occurring in these layers during cooling of structures after stop of the growth process caused by the difference in thermal expansion coefficients of W layer and substrate.

6. Conclusion

Thus, in this study using CVD method the thin superconducting layers of tungsten α-phase with low $T_c \sim 15$ mK were obtained for the first time, which proves the applicability of this deposition method for fabrication of low-temperature microcalorimeters and matrices on its basis. The layers of tungsten with hybrid $\alpha + \beta$-W phases could be of interest for studies at temperatures from 15 to 100 mK, however, these layers turned out to be poorly reproducible and demonstrated unstable values of T_c during repeated measurements. Therefore, currently no unambiguous conclusion can be made on the prospects of using such structures in microcalorimeters. Moreover, a method of electron-beam evaporation was used in this study to fabricate the superconducting layers of iridium, which may serve the ground for the formation of bi-layers with the superconducting junction temperature in the range 15–100 mK. The superconductivity was observed only for the thickest iridium layers of 135 nm, however, the specific density and resistivity for a much thinner layer of 45 nm are consistent with a bulk material. We suppose that this singularity of iridium thinner layers is explained by the influence of stresses arising in crystalline structure of the layers on silicon or sapphire substrates. Apparently, to provide the growth of thinner iridium superconducting layers we need to find appropriate sub-layers in the layer-substrate region to reduce the stresses in crystalline structure.

Funding

This study was carried out as part of the scientific program of the National Center for Physics and Mathematics (subject No. 8 „Hydrogen isotopes physics“). The equipment of the Center for Collective Use of Institute for Physics of Microstructures of Russian Academy of Sciences „Physics and Technology of Micro- and Nanostructures“ was used.

Conflict of interest

The authors declare that they have no conflict of interest.

References

[1] C. Chang, G. Wang. Transition edge sensors (TES) for photon detection. SNOWMASS 2021 (IF02), Seattle, WA. (July 18, 2022).
[2] Jurek Loebell. Setup of UHV System for the Production of Tungsten TES. Dissertation. (Tubingen 2016).
[3] A.H. Abdelhameed, G. Angloher, P. Bauer, A. Bento, E. Bertoldo, L. Canonica, D. Fuchs, D. Hauff, N. Ferreiro Iachellini, M. Mancuso, F. Petricca, F. Probst, J. Riesch, J. Rothe. J. Low Temper. Phys. https://doi.org/10.1007/s10909-020-02357
[4] A.E. Lita, D. Rosenberg, S. Nam, A.J. Miller, D. Balzar, L.M. Kaatz, R.E. Schwall. IEEE Transact. Appl. Supercond. **15**, *2*, 3528 (2005). DOI: 10.1109/TASC.2005.849033
[5] F.T.N. Vüllers, R. Spolenak. Thin Solid Films **577**, 26 (2015). http://dx.doi.org/10.1016/j.tsf.2015.01.030
[6] U. Nagel, A. Nowak, E. Kellner, H.-J. Gebauer, P. Colling, S. Cooper, D. Dummer, P. Ferger, M. Frank, P. Freund, G. Ferster, J. Igalson, A. Nucciotti, F. Probst, A. Rulofs, W. Sidel, L. Stodolsky. J. Low Temp. Phys. **93**, 543 (1993). https://doi.org/10.1007/BF00693473
[7] D.F. Bogorin, M. Galeazzi. J. Low Temp. Phys. **151**, 167 (2008). DOI: 10.1007/s10909-007-9622-4
[8] R. Hennings-Yeomans, C.L. Chang, J. Ding, A. Drobizhev, B.K. Fujikawa, S. Han, G. Karapetrov, Yu.G. Kolomensky, V. Novosad, T. O'Donnell, J.L. Ouellet, J. Pearson, T. Polakovic, D. Reggio, B. Schmidt, B. Sheff, V. Singh, R.J. Smith, G. Wang, B. Welliver, V.G. Yefremenko, J. Zhang. J. Appl. Phys. **128**, 154501 (2020). https://doi.org/10.1063/5.0018564
[9] V. Singh, M. Beretta, E.V. Hansen, K.J. Vetter, G. Benato, C. Capelli, B.K. Fujikawa, B. Schmidt, C.L. Chang, Yu.G. Kolomensky, B. Welliver, M. Lisovenko, G. Wang, V. Yefremenko, J. Zhang, L. Marini, W.K. Kwok, J. Pearson, U. Welp, V. Novosad. arXiv: 2210.15619v2 [physics.ins-det] 30 Oct 2022. Phys. Rev. Appl. **20**, 064017 (2023). https://doi.org/10.1103/PhysRevApplied.20.064017
[10] Gensheng Wang, Jeffrey Beeman, Clarence L. Chang, Junjia Ding, A. Drobizhev, B.K. Fujikawa, K. Han, S. Han, R. Hennings-Yeomans, Goran Karapetrov, Yury G. Kolomensky, Valentyn Novosad, T. O'Donnell, J.L. Ouellet, John Pearson, B. Sheff, V. Singh, S. Wagaarachchi, J.G. Wallig, Volodymyr G. Yefremenko. IEEE Transact. Appl. Supercond. **27**, *4*, 2100405 (2017). DOI: 0.1109/TASC.2016.2646373
[11] M. Golosov, V. Lozanov, N. Baklanova. Mater. Today: Proc. **25** (February, 2020). https://doi.org/10.1016/j.matpr.2019.12.088

Translated by T.Zorina